Stochastic sensitivity analysis of noise-induced suppression of firing and giant variability of spiking in a Hodgkin-Huxley neuron model

Irina Bashkirtseva,[1,*] Alexander B. Neiman,[2,†] and Lev Ryashko[1,‡]
[1]*Department of Mathematics, Ural Federal University, Pr. Lenina 51, Ekaterinburg, Russia*
[2]*Department of Physics and Astronomy, Ohio University, Athens, Ohio 45701, USA*
(Received 21 February 2015; published 29 May 2015)

We study the stochastic dynamics of a Hodgkin-Huxley neuron model in a regime of coexistent stable equilibrium and a limit cycle. In this regime, noise may suppress periodic firing by switching the neuron randomly to a quiescent state. We show that at a critical value of the injected current, the mean firing rate depends weakly on noise intensity, while the neuron exhibits giant variability of the interspike intervals and spike count. To reveal the dynamical origin of this noise-induced effect, we develop the stochastic sensitivity analysis and use the Mahalanobis metric for this four-dimensional stochastic dynamical system. We show that the critical point of giant variability corresponds to the matching of the Mahalanobis distances from attractors (stable equilibrium and limit cycle) to a three-dimensional surface separating their basins of attraction.

DOI: 10.1103/PhysRevE.91.052920 PACS number(s): 05.45.−a, 87.19.ln, 05.40.−a

I. INTRODUCTION

The phenomenon of multistability, i.e., the coexistence of several admissible stable states, is often observed in excitable neuronal systems. Coexistent stable states are represented by different types of attractors in the phase space of a system. For example, spiking neurons may possess coexistent quiescent (equilibrium) and tonic spiking states (limit cycle) [1], distinct periodic and chaotic spiking states [2], and tonic spiking and bursting states [3,4]. A given state can be reached if a system starts from a set of initial conditions within the state's basin of attraction. Otherwise, an external perturbation can be used to switch the system from one stable attractor to another.

With noise taken into account, phase trajectories of a system will likely hop between multiple stable states. In particular, Gaussian white noise may lead to global stability of a multistable system [5]. Important and challenging problems are to find the residence times that the system spends in each of its multistable states and its statistics, a critical value of noise intensity and control parameters at which noise-induced hopping becomes significant, and the overall statistics of noisy dynamics. Analytical treatment of such problems based on forward or backward Kolmogorov-Fokker-Planck equations becomes complicated for multidimensional systems, $n \geqslant 2$, and various approximations are commonly used [6–8]. For weak noise, asymptotic analyses based on the concept of quasipotential were developed [8,9], including the noise-perturbed limit cycle [10,11], stochastic excitable systems [12], escape problems [13–17], and nonlinear stability [18]. However, direct application of these approaches, e.g., to escape problems for systems with dimension $n > 2$, is made more difficult by complicated geometry and the structure of manifolds of saddle equilibrium and limit cycles separating basins of attraction [19].

The quasipotential gives exponential asymptotics for the stationary probability density. In the vicinity of the deterministic attractor, the first approximation of the quasipotential is a quadratic form [20], leading to a Gaussian approximation of the stationary probability density. The corresponding covariance matrix characterizes a stochastic sensitivity of the deterministic attractor: its eigenvalues and eigenvectors define the geometry of bundles of stochastic trajectories around the deterministic attractors. Gaussian distribution centered on an attractor can be viewed as a confidence ellipsoid, while a minimal distance from this ellipsoid to the boundary separating basins of attraction is proportional to the escape probability [21–24]. The appropriate measure for this distance is the so-called Mahalanobis distance [25], i.e., the distance from a point to a distribution.

Here we extend the method of the stochastic sensitivity function and Mahalanobis metrics to high-dimensional ($n \geqslant 3$) noise-perturbed systems for which a surface separating basins of attraction is unknown. In particular, we analyze the effect of noise-induced suppression of firing in the standard four-dimensional ($n = 4$) Hodgkin-Huxley model [26]. This effect occurs when the model is poised in a regime where a stable limit cycle, corresponding to a periodic sequence of action potentials, coexists with a stable equilibrium. This phenomenon was observed in an experiment [1] and was analyzed in several modeling studies [27–29]. An interesting observation is that at a critical value of injected current within the parameter range of bistability, the Hodgkin-Huxley neuron exhibits spiking with a giant variability of interspike intervals [27]. We apply the stochastic sensitivity analysis and the Mahalanobis metric to reveal the dynamical origin of this phenomenon.

This paper is organized as follows. In the next section, we describe the effect of noise-induced suppression of periodic firing and giant variability in the Hodgkin-Huxley and FitzHugh-Nagumo models by direct numerical simulations of corresponding stochastic differential equations. In Sec. III we introduce the method of statistical Mahalanobis distance and demonstrate its application to a two-dimensional (2D) FitzHigh-Nagumo system. We extend and apply our approach to the higher-dimensional 4D Hodgkin-Huxley model in Sec. IV.

*irina.bashkirtseva@urfu.ru
†Corresponding author: neimana@ohio.edu
‡lev.ryashko@urfu.ru

II. SUPPRESSION OF FIRING AND NOISE-INDUCED GIANT VARIABILITY

We use standard Hodgkin-Huxley (HH) equations (for details, see the Appendix),

$$C\dot{V} = -I_{\mathrm{Na}} - I_{\mathrm{K}} - I_{\mathrm{L}} + I_{\mathrm{ext}} + \sqrt{2D}\,\xi(t), \qquad (1)$$

with the control parameter being the injected (external) current, I_{ext}. The additive Gaussian white source $\xi(t)$ with intensity D mimics synaptic or extrinsic noise. Bifurcations of the deterministic model ($D = 0$) were studied in detail (see, e.g., [30]). For $I_{\mathrm{ext}} < I_{\mathrm{sn}} \approx 6.264\,81\ \mu\mathrm{A/cm}^2$, the HH system possesses a single stable equilibrium, which undergoes a subcritical Hopf bifurcation at $I_{\mathrm{ext}} = I_{\mathrm{hp}} \approx 9.770\,53\ \mu\mathrm{A/cm}^2$, and so for $I_{\mathrm{ext}} > I_{\mathrm{hp}}$ the only attractor is a stable limit cycle (SLC). The SLC and stable equilibrium, separated by unstable limit cycle(s), coexist in the bistability region, $I_{\mathrm{sn}} < I_{\mathrm{ext}} < I_{\mathrm{hp}}$. The SLC undergoes a saddle-node bifurcation at $I_{\mathrm{ext}} = I_{\mathrm{sn}}$. Additional bifurcations of saddle limit cycles occur within the bistability region: for $7.846\,47 < I_{\mathrm{ext}} < 7.921\,81$, the stable equilibrium and SLC are separated apparently by three unstable cycles [30]. Furthermore, near $I_{\mathrm{ext}} = 7.921\,98$, a chaotic regime has been documented in the narrow parameter interval of length less than 10^{-5} [30]. We focus on weak noise effects on the spiking dynamics of the HH system in the bistability region, $I_{\mathrm{sn}} < I_{\mathrm{ext}} < I_{\mathrm{hp}}$.

Sequences of spike times, t_k, of the stochastic HH model were recorded as moments of crossing a threshold of 20 mV by the rising phase of the action potential. The corresponding sequence of interspike intervals (ISIs) is $\tau_k = t_k - t_{k-1}$. Stochastic dynamics was quantified by statistics of the ISIs, such as the probability density function (pdf) of ISIs, the mean ISI, $\langle\tau\rangle$, and the coefficient of variation (CV), C_V, defined as the ratio of the ISIs' standard deviation to the mean ISI. For a noiseless periodic spike train, $C_V = 0$, while $C_V = 1$ for a Poisson spike train. The CV values greater than 1 thus correspond to a point process that is more variable than a Poisson process. The mean firing rate is reciprocal to the mean ISI, $\langle f\rangle = 1/\langle\tau\rangle$. In addition, we calculated the power spectral density $S(f)$ (PSD) of the corresponding spike train, $y(t) = \sum_{k=1}^{N(t)} \delta(t - t_k)$, where $N(t)$ is the number of spikes in $(0, t]$. The power at zero frequency is related to the effective diffusion constant of the spike counts, $N(t)$ [31,32],

$$S(f = 0) = \lim_{t\to\infty} \frac{\langle N^2(t)\rangle - \langle N(t)\rangle^2}{t},$$

which serves as a measure of spike count variability. For a renewal point process, such as spiking of the HH model with white noise, the effective diffusion constant is related to the CV and the mean firing rate as [32]

$$D_{\mathrm{eff}} = (C_V)^2\langle f\rangle. \qquad (2)$$

In numerical simulations, we collected at least 10^6 ISIs, and at least 10^2 transitions between quiescent and spiking states of the neuron model, which required very lengthy simulations for small values of noise intensity.

Figure 1 shows voltage traces of the HH model for three distinct regimes: (i) the excitable regime, $I_{\mathrm{ext}} = 6\ \mu\mathrm{A/cm}^2$, in which the deterministic system possesses a single stable equilibrium state; (ii) the bistable regime, $I_{\mathrm{ext}} = 8\ \mu\mathrm{A/cm}^2$,

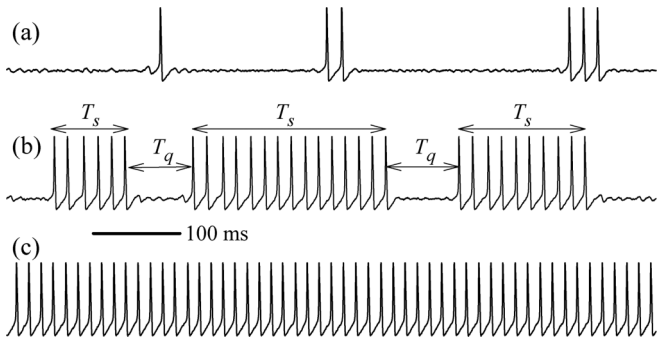

FIG. 1. Voltage traces of the stochastic HH model for three distinct regimes: (a) excitable, $I_{\mathrm{ext}} = 6\,\mu\mathrm{A/cm}^2$; (b) bistable, $I_{\mathrm{ext}} = 8\,\mu\mathrm{A/cm}^2$; and (c) single limit cycle, $I_{\mathrm{ext}} = 11\,\mu\mathrm{A/cm}^2$; $D = 0.3$ [$\mathrm{kHz}(\mu\mathrm{A/cm}^2)^2$] . In panel (b), T_s and T_q indicate the durations of spiking and quiescence epochs, respectively.

characterized by the coexistence of stable equilibrium and the stable limit cycle oscillations separated by an unstable limit cycle; and (iii) the single oscillatory regime, $I_{\mathrm{ext}} = 11\ \mu\mathrm{A/cm}^2$, whereby the system possesses a single stable limit cycle and unstable equilibrium. Figure 2 shows the probability density functions (pdfs) of ISIs (a) and PSDs (b) for these regimes. In the excitable regime, weak noise induces extremely sparse and short bursts of action potentials, Fig. 1(a). The corresponding pdf of ISIs, Fig. 2(a1), shows multiple peaks and a very long tail that extends for ISI longer than 10^5 ms. Note that these long ISIs correspond to intervals between the last spike in a burst and the next noise-elicited spike. The main peak corresponds to the ISIs within an oscillatory burst, and smaller peaks represent spike skipping by subthreshold oscillations of the membrane potential [27,33]. The corresponding PSD [black line in Fig. 2(b)] shows a broad peak corresponding to the main peak in the ISI distribution and its higher harmonics. The bistability regime is characterized by intermittent patterns of trains of periodic firing and quiescence [Fig. 1(b)], which can be characterized by the average durations of oscillating spiking, T_s, and quiescent, T_q, epochs. This presumably corresponds to noise-induced switching between limit cycle oscillations and a random walk around stable equilibrium [1,27,29], and it is reflected by a significantly smaller tail for long ISIs in the corresponding pdf, Fig. 2(a2). A higher degree of periodicity is reflected by a sharp peak in the PSD [Fig. 2(b)] at a frequency close to the mean firing rate of the neuron. A sharp peak at zero frequency reflects the intermittent nature of oscillating and quiescent epochs. Finally, the single oscillatory regime is characterized by a sharp unimodal ISI distribution, Fig. 2(a3), and sharply peaked PSD with no significant power at low frequencies.

Figure 3 displays the statistics of firing of a noisy HH neuron versus injected current. The mean firing rate, $\langle f\rangle$ [Fig. 3(a)], shows a crossover point at $I_{\mathrm{ext}} = I_{\mathrm{cr}} \approx 8\ \mu\mathrm{A/cm}^2$, where $\langle f\rangle$ depends weakly on noise intensity. For $I_{\mathrm{ext}} < 8$, the mean firing rate increases with D, while it does the opposite for $I_{\mathrm{ext}} > 8$. The average duration of the oscillatory spiking epochs, $\langle T_s\rangle$, increases with I_{ext}, and the average duration of the quiescent epochs, $\langle T_q\rangle$, decreases with I_{ext}, as Fig. 3(b) indicates. The average residences of the system in oscillatory spiking and

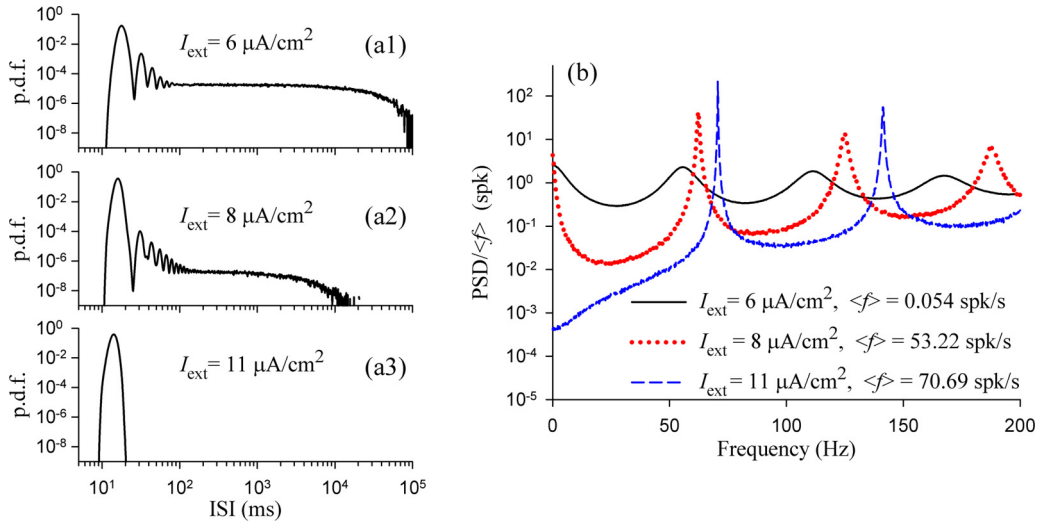

FIG. 2. (Color online) Statistics of spike trains generated by the stochastic HH model for the indicated values of the injected current, I_{ext}. (a1)–(a3) Probability density function (pdf) of ISIs. (b) PSD normalized to the mean firing rate of the neuron. Mean firing rates are indicated in the figure legend. The noise intensity was $D = 0.05$ for $I_{ext} = 8$ and $I_{ext} = 11$ μA/cm^2 and $D = 0.1$ for $I_{ext} = 6$ μA/cm^2. The units of noise intensity, D, are [kHz(μA/cm^2)^2] .

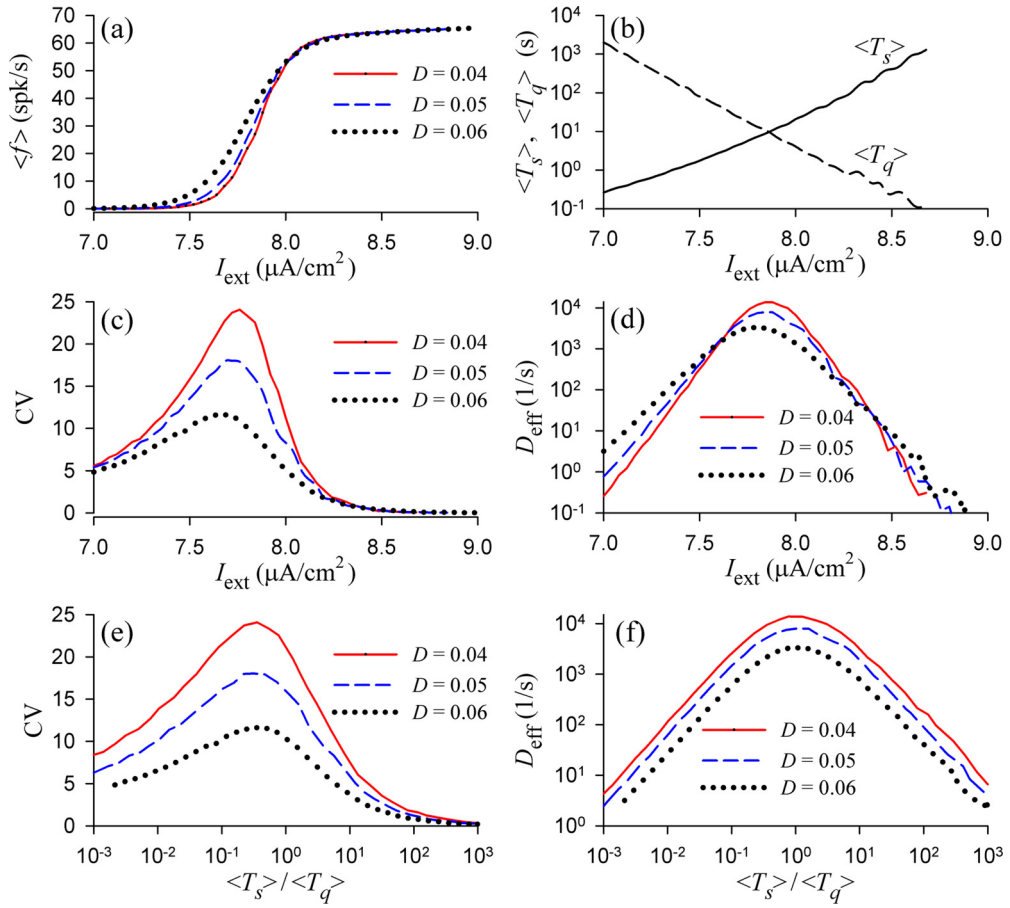

FIG. 3. (Color online) Statistics of the HH neuron firing vs injected current, I_{ext}. (a) Mean firing rate, $\langle f \rangle$, vs I_{ext} for the indicated values of noise intensity D. (b) Mean durations of spiking ($\langle T_s \rangle$, solid line) and quiescent ($\langle T_q \rangle$, dashed line) epochs vs I_{ext} for $D = 0.04$. (c) and (d) Coefficient of variation, CV, and effective diffusion constant D_{eff} (2), vs I_{ext} for the indicated values of D. Panels (e) and (f) show the same data as (c) and (d), except that CV and D_{eff} are plotted vs the relative average duration of the HH neuron in its oscillatory spiking and quiescent states, $\langle T_s \rangle / \langle T_q \rangle$. The units of noise intensity, D, are [kHz(μA/cm^2)^2].

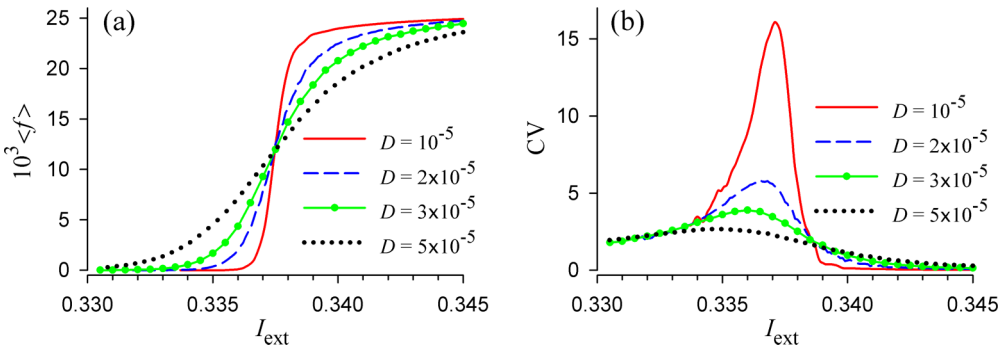

FIG. 4. (Color online) Mean firing rate (a) and the CV (b) of the stochastic FHN model vs injected current I_{ext} for the indicated values of noise intensity.

quiescent regimes match at $I_{ext} \approx 7.86$ for $D = 0.04$. The CV versus injected current [Fig. 3(b)] shows a maximum whose position is close to the crossover point in Fig. 3(a): a giant ISI variability with CV close to 24 occurs for weak noise, $D = 0.04$, and $I_{ext} \approx 7.8$. The variability of spike count quantified by the effective diffusion constant, D_{eff} (2), shows a similar dependence, reaching its maximum at $I_{ext} \approx 7.85$ for $D = 0.04$. The above observations indicate that spiking variability is maximal when the neuron resides equally in its spiking and quiescent states. This is further demonstrated in Figs. 3(e) and 3(f) showing variability measures versus the relative average duration of the system in oscillatory spiking and quiescent states. In particular, Fig. 3(f) indicates that the spike count variability, D_{eff}, peaks at $\langle T_s \rangle / \langle T_q \rangle \approx 1$, i.e., when the system resides on average equally in its spiking and quiescent states. We note that the observed effect of giant spiking variability and especially the behavior of the diffusion constant in Figs. 3(d) and 3(e) is akin to the phenomenon of giant diffusion of active Brownian particles whose velocities are subjected to a force drawn from an effective double-well potential [34]. The giant diffusion occurs for a critical asymmetry of the effective potential, and the effective diffusion constant of particles is maximal for the symmetric effective potential, which refers to equal average residence of particles' velocities within the effective potential wells. Similarly, giant spike count variability in the stochastic HH model occurs when the residence of the system in its quiescent and oscillatory spiking states become comparable, attaining its maximum value when the average durations of quiescent and oscillatory spiking epochs are equal.

Similar stochastic dynamics with giant ISI variability was observed for the 2D Morris-Lecar system [27] and also for the FitzHugh-Nagumo (FHN) model, which we demonstrate in Fig. 4. The FHN model is given by

$$\dot{V} = V - \frac{V^3}{3} - w + I_{ext} + \sqrt{2D}\,\xi(t),$$
$$\dot{w} = 0.1(V + 0.7 - 0.8w). \qquad (3)$$

For the deterministic FHN model, $D = 0$, a saddle-node bifurcation of the limit cycle occurs at $I_{ext} = I_{sn} = 0.332\,322\,8$ and a subcritical Hopf bifurcation occurs at $I_{hp} = 0.341\,067\,2$. For $I_{sn} < I_{ext} < I_{hp}$, the FHN model is bistable with coexisting stable equilibrium and the stable limit cycle. With noise added, the FHN model shows crossover behavior of the mean firing rate similar to that of the Hodgkin-Huxley system, i.e., for $I_{ext} = I_{cr} \approx 0.337$ the mean firing rate depends weakly on noise intensity, and the resulting sequences of ISIs show giant variability with $C_V > 15$ for weak noise (Fig. 4).

III. STOCHASTIC SENSITIVITY ANALYSIS AND GEOMETRICAL ARRANGEMENT OF ATTRACTORS

The fact that the stochastic dynamics of both models is almost invariant with respect to variation of noise intensity at the critical crossover point in Figs. 3 and 4(a) means that it is related to the geometrical arrangements of stable attractors and separatrices in the phase space of deterministic systems. The point of giant variability corresponds approximately to equal residency of phase trajectories in the basins of attraction of stable equilibrium and the stable limit cycle. The residence time of phase trajectories in the basin of attraction depends on two factors. First, there is a geometrical arrangement of an attractor and its basin of attraction, e.g., the larger the distance is between an attractor and the separatrix isolating its basin of attraction, the longer is the residence time of phase trajectories in the basin. Second, there is a sensitivity of attractors to random perturbations: the higher this stochastic sensitivity is, the higher is the probability to escape from the basin of attraction, and thus the shorter is the residence time [8,15].

Figure 5 shows the attractors of the deterministic FHN system, and it also indicates the positions of minimal Euclidean distances from stable attractors to an unstable limit cycle, which plays the role of the separatrix. The unstable limit cycle for the FHN and HH models can be calculated and continued numerically using parameter-continuation software, such as MATCONT (used in this study) and AUTO [35,36]. With the increase of the control parameter, I_{ext}, the Euclidean distance, d_E, from the stable to unstable cycles grows, while d_E from the equilibrium to unstable cycle decreases, as Fig. 6 shows. Both these Euclidean distances coincide at $I_{ext} \approx 0.34$, which is far off from the crossover point of $I_{ext} \approx 0.337$ in Fig. 4(a), obtained by direct numerical simulation of the stochastic FHN model. This indicates that the mere geometrical arrangement of attractors and the separatrix (the unstable limit cycle in the case of the FHN model) does not explain the stochastic dynamics at $I_{ext} = I_{cr}$, and thus the second factor mentioned above, i.e., the stochastic sensitivity of attractors, should be taken into account.

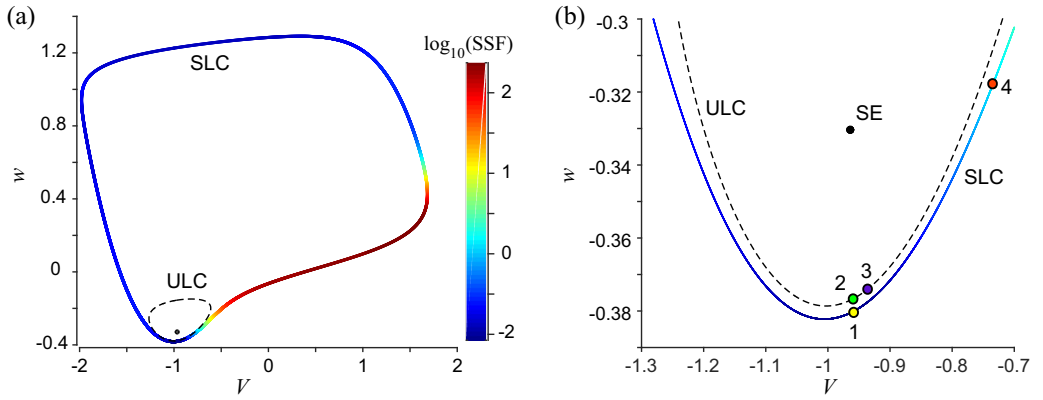

FIG. 5. (Color online) Geometry of attractors of the Fitzhugh-Nagumo model for $I_{\text{ext}} = 0.335$. The stable limit cycle (SLC) is color-coded according to its stochastic sensitivity function (SSF). The unstable (saddle) limit cycle (USL) is shown by the dashed line, and stable equilibrium (SE) is shown by the black circle. Panel (b) shows an expanded region of panel (a). Yellow circle 1 on the stable limit cycle indicates the minimal Euclidean distance from the stable to the unstable limit cycle; green circle 2 on the unstable limit cycle marks the minimal Euclidean distance from stable equilibrium to the unstable limit cycle; red circle 4 indicates the minimal Mahalanobis distance from the stable to the unstable limit cycle; and blue circle 3 on the unstable limit cycle corresponds to the minimal Mahalanobis distance from stable equilibrium to the unstable limit cycle.

The stochastic sensitivity function (SSF) is an asymptotic characteristics of noisy attractors of a dynamical system. For weak noise, it allows us to approximate a spread of random states around these attractors. The SSF technique was elaborated on for systems with equilibria and limit cycles in [21–23]. A brief review of this technique is presented in the Appendix. In essence, for weak noise the probability density-of-states variable, $\mathbf{x}$, is approximated by a Gaussian distribution centered on the stable attractor of the system, $\mathbf{x} = \bar{\mathbf{x}}$,

$$\rho_G(\mathbf{x},\varepsilon;\bar{\mathbf{x}}) \;=\; N \exp\left[-\frac{(\mathbf{x}-\bar{\mathbf{x}})^{\top}\mathbf{Q}^{-1}(\mathbf{x}-\bar{\mathbf{x}})}{2\varepsilon^2}\right], \qquad (4)$$

where ε is a small parameter corresponding to noise intensity and N is a normalization constant. In Eq. (4), $\mathbf{Q}$ is the stochastic sensitivity matrix or function (SSF) of the attractor $\bar{\mathbf{x}}$, and it is determined by an algebraic equation (A5) for a stable equilibrium or by the differential Lyapunov equation (A6) for a stable limit cycle. Eigenvalues, λ_i, and eigenvectors, $\mathbf{v_i}$, of the SSF define a geometric configuration of the confidence ellipsoids, i.e., the variance of random states around the stable attractor. For a stable limit cycle, the SSF depends on time along the limit cycle and thus its eigenvalues and eigenvectors. They form a family of confidence ellipsoids around the stable limit cycle [21–23]. For a slow-fast dynamical system, such as the FHN and HH neuron models, the eigenvalues of SFF may vary nonuniformly along the limit cycle. This is demonstrated for the FHN model in Fig. 7(a), which shows that the SSF of the stable limit cycle is large on the rising phase of the voltage, takes its maximum at the maximum of V, and then rapidly drops (compare with Fig. 5). This strikingly wide dynamical range of stochastic sensitivity reflects nonuniform motion in the phase space of this slow-fast dynamical system. The stochastic sensitivity diverges at the bifurcation points as Fig. 7(b) indicates: the SSF of the stable equilibrium diverges at $I_{\text{ext}} = I_{\text{hp}} = 0.341\,067\,2$, i.e., at subcritical Hopf bifurcation; the SSF of the limit cycle diverges at the saddle-node bifurcation, $I_{\text{ext}} = I_{\text{sn}} = 0.332\,322\,8$. Furthermore, the largest eigenvalue of the SSF of stable equilibrium and the maximal value of the largest eigenvalue of the SSF of the stable limit cycle match at $I_{\text{ext}} \approx 0.337$, indicating that at this parameter value, both attractors are equally sensitive to noise perturbations.

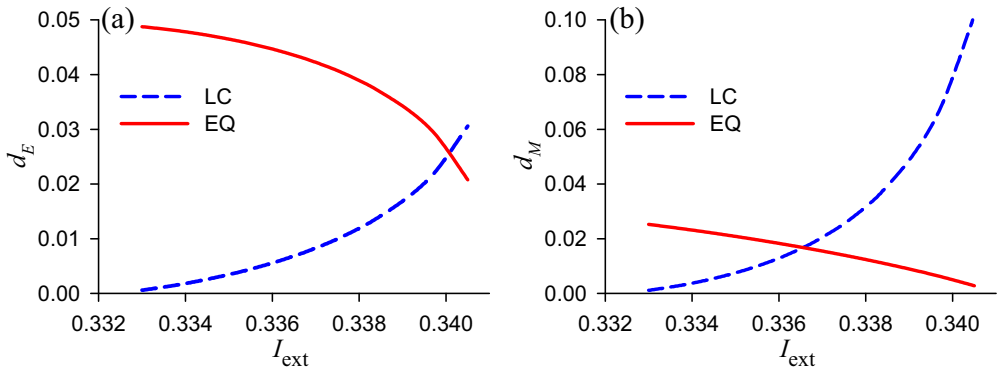

FIG. 6. (Color online) Minimal (a) Euclidean, d_E, and (b) Mahalanobis, d_M, distances from the attractors to the unstable limit cycle vs I_{ext} for the FitzHugh-Nagumo model. On both panels the blue dashed line shows the minimal distance between stable and unstable limit cycles; the red solid line corresponds to the minimal distance from stable equilibrium to the unstable limit cycle.

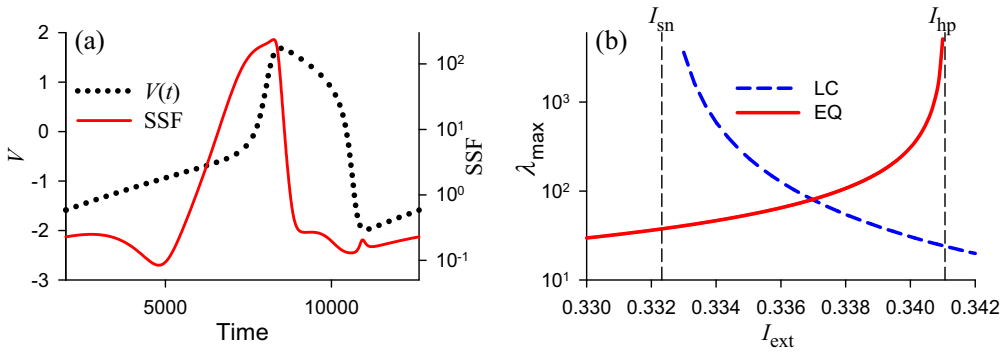

FIG. 7. (Color online) Stochastic sensitivity of attractors in the FitzHugh-Nagumo model. (a) Dependence $V(t)$ (black dotted line, left axis) and stochastic sensitivity function (SSF, red solid line, right axis) along the stable limit cycle for $I_{ext} = 0.335$. (b) Largest eigenvalue of SSF of the stable equilibrium (EQ, red solid line) and the maximum value of the largest eigenvalue of SSF of the stable limit cycle (LC, blue dashed line) vs I_{ext}. Vertical dashed lines show the locations of subcritical Hopf bifurcation of stable equilibrium (I_{hp}) and saddle-node bifurcation of the stable limit cycle (I_{sn}).

The color-coded stable cycle in Fig. 5 indicates that the highest stochastic sensitivity does not correspond to the smallest Euclidean distances to the separatrix. On the contrary, the SSF of the stable limit cycle is small in the region of the smallest Euclidean distance to the separatrix. Thus, two factors contributing to the probability to escape from the basin of attraction of the stable limit cycle are in competition. Here we propose to use the Mahalanobis distance, a metric widely used in cluster and discriminant analyses [37]. The Mahalanobis distance measures the distance between a point $\mathbf{x}$ and a distribution. In stochastic sensitivity analysis, we approximate the probability density by a Gaussian distribution (4) centered at a stable attractor, $\bar{\mathbf{x}}$, and the Mahalanobis distance from a point $\mathbf{x}$ to the distribution of phase trajectories around a noisy perturbed attractor is given by

$$d_M(\mathbf{x};\bar{\mathbf{x}}) = \sqrt{(\mathbf{x}-\bar{\mathbf{x}})^{\top}\mathbf{Q}^{-1}(\mathbf{x}-\bar{\mathbf{x}})}, \tag{5}$$

where $\mathbf{Q}$ is the stochastic sensitivity matrix, and so the Gaussian approximation (4) can be written in terms of $d_M(\mathbf{x};\bar{\mathbf{x}})$ as

$$\rho(\mathbf{x}) = N\exp\left[-\frac{d_M^2(\mathbf{x};\bar{\mathbf{x}})}{2\varepsilon^2}\right]. \tag{6}$$

The Mahalanobis distance combines both the geometric distance from the attractor and its sensitivity to noise, which makes this metric a natural tool for the quantitative analysis of noise-induced transitions. In a multistable case, such as the one shown in Fig. 5, the Mahalanobis metrics allows us to estimate a "preference" of attractors in the stochastic dynamics of the system, when the random trajectory passes from one attractor to another. For any basin of attraction and weak noise, the Mahalanobis distance from the corresponding attractor to the separatrix is related to the residence time of the system in the basin: the larger the Mahalanobis distance is, the longer is the residence time in the basin. For the example of bistability in the FHN model, we calculate the Mahalanobis distances from stable attractors ($\bar{\mathbf{x}}$ is taken at equilibrium or on the limit cycle) to the separatrix ($\mathbf{x}$ is taken at the unstable limit cycle), and then we compute their minimal values. Figure 6(b) shows the dependence of Mahalanobis distances from coexisting equilibrium and the stable limit cycle to the separatrix for the FHN model for various values of I_{ext}. The Mahalanobis distances match for $I_{ext} = I_{cr} \approx 0.337$, which corresponds well to the crossover point in Fig. 4(a). At this point, the average residence time of the system in the basin of attraction of equilibrium and the stable limit cycle are equal. This leads to a weak dependence of the mean firing rate on the noise intensity and to large values of CV (giant variability), Fig. 4(b). We stress that the use of stochastic sensitivity analysis and Mahalanobis metrics requires analysis of an essentially deterministic system, thus allowing predictions of noise-induced transitions without direct and lengthy numerical simulation of stochastic dynamics.

IV. STOCHASTIC SENSITIVITY ANALYSIS OF THE NOISY HODGKIN-HUXLEY MODEL

Stochastic sensitivity analysis can be extended to a higher-dimensional ($n = 4$) Hodgkin-Huxley model. However, the use of the Mahalanobis distances from stable attractors to the separatrix is complicated by the fact that the separatrix between the stable equilibrium and the stable limit cycle is a 3D surface that is hard to compute [30]. An unstable limit cycle (that can be computed using continuation software) is embedded into the separatrix surface.

Figure 8 shows a 2D projection of HH attractors and an unstable limit cycle for $I_{ext} = 8\ \mu\text{A/cm}^2$. We start with SSF analysis of stochastic dynamics near the stable equilibrium. Eigenvalues λ_i ($i = 1,2,3,4$) of the SSF, $\mathbf{Q}$, are simple scalar characteristics of the distribution of random states around the equilibrium. For a fixed noise strength and fiducial probability, a difference in λ_i reflects a spatial nonuniformity of the dispersion of these states in the direction of the eigenvectors $\mathbf{v_i}$, as the sizes of the semiaxes of confidence ellipsoids are proportional to $\sqrt{\lambda_i}$. The dependence of λ_i vs injected current, I_{ext}, is shown in Fig. 9(a). The main feature is the dominance of the largest eigenvalues λ_1 (shown by a solid black line), which is two orders of magnitudes larger than the rest of the eigenvalues and diverges at the Andronov-Hopf bifurcation, $I_{ext} = I_{hp}$ [solid red line in Fig. 11(a)]. This means that the

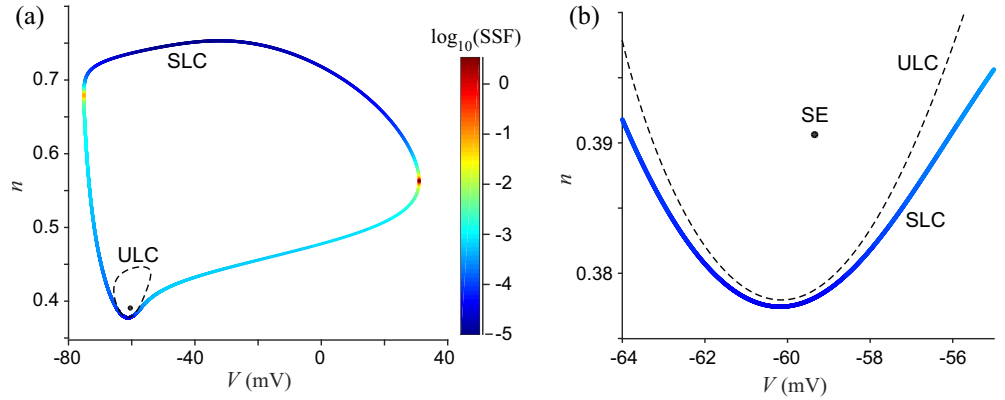

FIG. 8. (Color online) Two-dimensional projection of attractors of the Hodgkin-Huxley model for $I_{ext} = 8\ \mu A/cm^2$. The stable limit cycle (SLC) is color-coded according to the maximum eigenvalue of its stochastic sensitivity function (SSF). The unstable (saddle) limit cycle (USL) is shown by the dashed line, and stable equilibrium (SE) is shown by the black circle. Panel (b) shows an expanded region of panel (a).

confidence ellipsoid is elongated in the direction of the eigenvector $\mathbf{v}_1$ and extremely narrow in all other directions. Thus, the eigenvector $\mathbf{v}_1$ localizes the main direction for deviations of random trajectories from the equilibrium, providing the direction in which the intersection with the separatrix surface is to be expected. In these circumstances, the minimum distance from the equilibrium to all points on the separatrix, S, can be approximated by the Mahalanobis distance to the separatrix S along the eigenvector $\mathbf{v}_1$,

$$d_M = \min_{\mathbf{x}\in S} d_M(\mathbf{x};\bar{\mathbf{x}}), \tag{7}$$

where $\bar{\mathbf{x}}$ are coordinates of the stable equilibrium, $\bar{\mathbf{x}} = \{\bar{V},\bar{m},\bar{h},\bar{n}\}$.

A similar approach is applied to the analysis of a noisy perturbed limit cycle. In this case, the SSF matrix is periodic in time, $\mathbf{Q}(t) = \mathbf{Q}(t+T)$, where T is the period of a stable limit cycle. The Mahalanobis distance $d_M(\mathbf{x};\bar{\mathbf{x}})$ is also a periodic function of time. Eigenvalues $\lambda_i(t)$ $(i = 1,2,3,4)$ of $\mathbf{Q}(t)$ characterize the distribution of random states in the Poincaré section Π_t near the point $\bar{\mathbf{x}}(t)$ of the cycle. It follows from the singularity of $\mathbf{Q}(t)$ that $\lambda_4(t) = 0$. Other eigenvalues, $\lambda_1(t) > \lambda_2(t) > \lambda_3(t) > 0$, are shown in Fig. 9(b).

Here, similar to the FHN model, we observe a significant overfall of values along the cycle. The maximal stochastic sensitivity (maximal value of the largest eigenvalue, λ_1) occurs at the peak value of the membrane potential, corresponding to the maximal open probability of the sodium ion channels [Fig. 9(b), upper panel]. This peak is followed by a rapid decrease of λ_1, and stochastic sensitivity of the stable limit cycle is small in a region close to the unstable limit cycle and stable equilibrium (Fig. 8). Figure 10 shows the excellent correspondence between the variance of the phase trajectories around the stable limit cycle estimated with the SSF matrix and by direct numerical simulation. The theoretical value of this variance is given by the trace of the SSF matrix on the stable limit cycle, $\mathrm{var}(t) = 2D\,\mathrm{tr}[\mathbf{Q}(t)]$. In numerical simulations, we constructed a set of Poincaré sections along the stable limit cycle (22 in Fig. 10), collected 10^4 intersections of phase trajectories in each section, and calculated the variance of the resulting points.

The dependence of the largest eigenvalues of SSF for the stable equilibrium and the maximum value of the largest eigenvalue of SSF for the stable limit cycle versus injected current is shown in Fig. 11(a). Closely akin to the FHN model, the largest eigenvalues diverge at the bifurcation

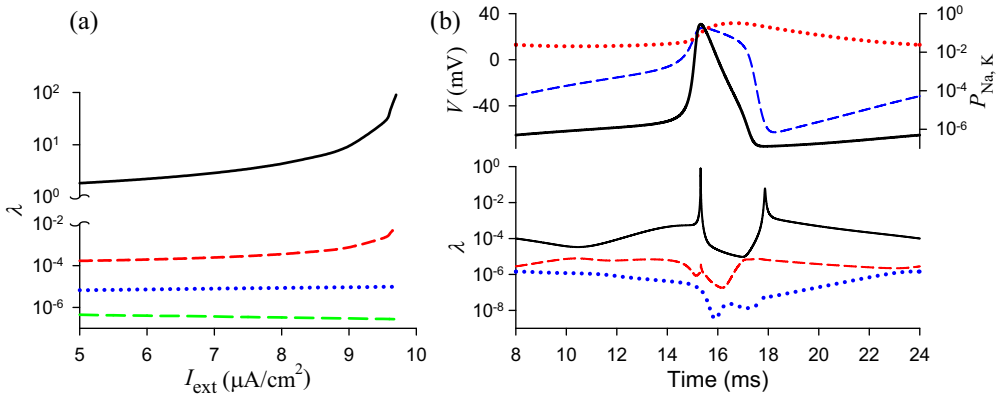

FIG. 9. (Color online) Stochastic sensitivity of stable attractors of the Hodgkin-Huxley system. (a) Eigenvalues of the SSF matrix for the stable equilibrium vs I_{ext}. (b) Stochastic sensitivity of a stable limit cycle for $I_{ext} = 8\ \mu A/cm^2$. Upper panel: membrane potential, $V(t)$ (solid black line, left vertical axis), and open probability of sodium, $P_{Na} = m^3h$ (dashed blue line, right y axis), and potassium, $P_K = n^4$ (dotted red line, right y axis), ion channels during one period of the stable limit cycle. Lower panel: eigenvalues of the SSF matrix along the limit cycle.

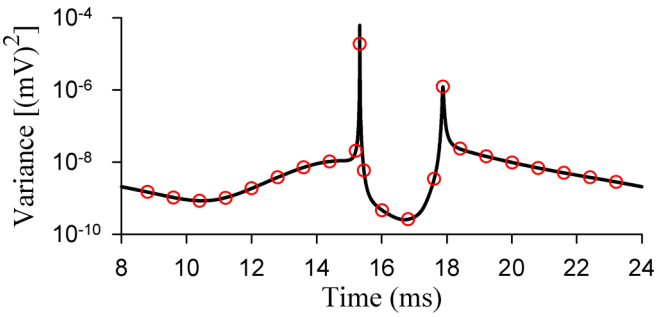

FIG. 10. (Color online) Comparison of the variance of phase trajectories of a stochastic HH neuron around its stable limit cycle obtained using the SSF analysis (solid line) and by direct numerical simulation (circles). The parameters are $I_{ext} = 8\ \mu A/cm^2$, $D = 10^{-5}$ [kHz$(\mu A/cm^2)^2$] .

points: at Andronov-Hopf bifurcation, $I_{ext} = I_{hp}$, for the stable equilibrium, and at saddle-node bifurcation, $I_{ext} = I_{sn}$, for the stable limit cycle. Furthermore, the largest eigenvalues coincide at $I_{ext} \approx 7.8\ \mu A/cm^2$.

The minimal Mahalanobis distance between the stable limit cycle and the separatrix can be approximated in a manner similar to the case of stable equilibrium. Due to the domination of the largest eigenvalue, $\lambda_1(t)$, the corresponding eigenvector $\mathbf{v}_1(t)$ localizes the main direction for deviations of random trajectories from the stable limit cycle. Consequently, the minimal Mahalanobis distance, d_M, from the stable cycle to all points on the separatrix surface, S, is approximated by the distance from the stable cycle to the separatrix surface, S, in the direction of the leading eigenvector $\mathbf{v}_1(t)$,

$$d_M = \min_{t\in[0,T),\ \mathbf{x}\in S} d_M[\mathbf{x},\bar{\mathbf{x}}(t)], \tag{8}$$

where $\bar{\mathbf{x}}$ is taken on the stable limit cycle, $\bar{\mathbf{x}}(t) = \{\bar{V}(t),\bar{m}(t),\bar{h}(t),\bar{n}(t)\}$.

The dependences of the minimal Mahalanobis distances from stable attractors to the separatrix on injected current are shown in Fig. 11(b). The Mahalanobis distance from the stable limit cycle to the separatrix vanishes at $I_{ext} = I_{sn}$, i.e., at saddle-node bifurcation of the limit cycle, and then increases with I_{ext}. The Mahalanobis distance from the equilibrium to the separatrix vanishes at subcritical Andronov-Hopf bifurcation, $I_{ext} = I_{hp}$, and increases for decreasing values of I_{ext}. Both distances match at $I_{ext} = 8.0\ \mu A/cm^2$, i.e., at the critical value of injected current, which corresponds to the crossover point of the mean firing rate and giant variability observed in direct numerical simulations of the stochastic HH model (Fig. 3). For $I_{ext} < I_{cr}$, the Mahalanobis distance for the equilibrium is larger than that for the stable limit cycle. Hence, random trajectories reside longer in the basin of attraction of the equilibrium. For $I_{ext} > I_{cr}$, the Mahalanobis distance for the limit cycle is larger, and so random trajectories "prefer" the basin of attraction of the stable limit cycle. For $I_{ext} = I_{cr}$, both basins are equiprobable.

V. CONCLUSION

We have developed an approach for analysis of the dynamics of multidimensional multistable excitable systems perturbed by weak noise. This method uses the stochastic sensitivity functions technique and the Mahalanobis metric to study noise-induced transitions between coexisting attractors. We addressed an issue of estimation of the Mahalanobis distance from a distribution on the attractor to an unknown separatrix surface that isolates its basin of attraction. In essence, we measured the Mahalanobis distance along the direction prescribed by the leading eigenvector of the stochastic sensitivity matrix.

We applied this method to the analysis of noise-induced hopping between periodic firing and quiescence in the stochastic Hodgkin-Huxley neuron model. We have shown the existence of a critical value of the control parameter (injected current I_{ext}) at which the mean firing rate is invariant with respect to variation of weak noise intensity, while the variability of the interspike intervals and spike count becomes extremely large. This regime is characterized by intermittent epochs of oscillatory spiking and quiescence with equal average durations. The observed phenomenon of giant spiking variability is similar to the effect of giant diffusion of active

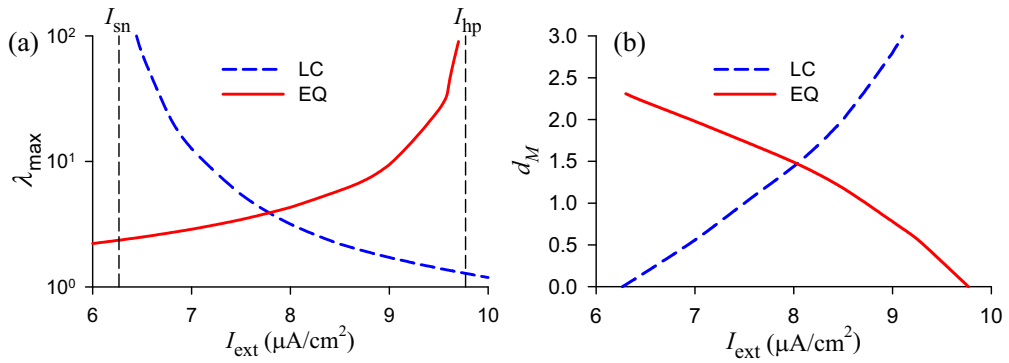

FIG. 11. (Color online) Stochastic sensitivity and minimal Mahalanobis distances for the Hodgkin-Huxley model vs injected current. (a) Largest eigenvalue of SSF of the stable equilibrium (EQ, red solid line) and the maximum value of the largest eigenvalue of SSF of the stable limit cycle (LC, blue dashed line) vs I_{ext}. Vertical dashed lines show the locations of subcritical Hopf bifurcation of stable equilibrium (I_{hp}) and saddle-node bifurcation of the stable limit cycle (I_{sn}). (b) Minimal Mahalanobis distances, d_M, from stable attractors to separatrix surface vs I_{ext}. The blue line (LC) shows the minimal Mahalanobis distance between stable limit cycles and the separatrix; the red line (EQ) corresponds to the minimal Mahalanobis distance between stable equilibrium and the separatrix.

Brownian particles [34,39–41]: the effective diffusion constant of active Brownian particles is maximal, when their velocities are subjected to a force drawn from a symmetric effective potential, so that the particles' velocities reside on average equally long in the effective potential wells.

We showed that a mere geometrical arrangement of stable attractors and separatrices does not provide an adequate explanation of this phenomenon, and so the sensitivity of the system to noise perturbations must be taken into account. The Mahalanobis distance, which combines geometrical and stochastic sensitivity aspects of the dynamics, allows for a proper explanation of the critical point, which refers to the parameter value at which minimal Mahalanobis distances from stable attractors to the separatrix coincide.

The approached described here can be applied to various multidimensional neuronal models and various kinds of multistability perturbed by *weak* noise, providing that coexisting attractors are exponentially stable. Furthermore, the Mahalanobis metric can be used in the analysis of the noise-induced exits of random trajectories beyond the bounds of the basin of attraction. The most probable zone where random trajectories cross the separatrix is located in the region closest to the attractor in the Mahalanobis metric. Thus, this zone on the separatrix represents a "transition bridge" for trajectories escaping from one attractor to another. Likewise, a zone on a stable limit cycle closest to the separatrix in the Mahalanobis sense represents a transition bridge for trajectories escaping from the limit cycle to another attractor.

ACKNOWLEDGMENTS

The authors thank Benjamin Lindner and Felix Droste for stimulating discussions. I.B. and L.R. acknowledge support by the Russian Foundation for Basic Research (Grant No. 14-01-00181). A.N. gratefully acknowledges the support of NVIDIA Corporation with the donation of the Tesla K40 GPU used for this research.

APPENDIX

1. Hodgkin-Huxley model

The Hodgkin-Huxley model is given by

$$\begin{aligned} C\dot{V} &= I_{\text{ext}} - \bar{g}_{\text{K}} n^4 (V - V_k) - \bar{g}_{\text{Na}} m^3 h (V - V_{\text{Na}}) \\ &\quad - g_{\text{L}} (V - V_{\text{L}}) + \sqrt{2D}\xi(t), \\ \dot{m} &= \alpha_m(V)(1-m) - \beta_m(V) m, \\ \dot{n} &= \alpha_n(V)(1-n) - \beta_n(V) n, \\ \dot{h} &= \alpha_h(V)(1-h) - \beta_h(V) h. \end{aligned} \tag{A1}$$

Here, C is the membrane capacitance, V is the membrane potential, I_{ext} is the applied (injected) current, m,n,h are the gating variables,

$$\begin{aligned} \alpha_m(V) &= \frac{0.1(V+40)}{1-\exp[-(V+40)/10]}, \\ \beta_m(V) &= 4\exp[-(V+65)/18], \\ \alpha_n(V) &= \frac{0.01(V+55)}{1-\exp[-(V+55)/10]}, \\ \beta_n(V) &= 0.125\exp[-(V+65)/80], \\ \alpha_h(V) &= 0.07\exp[-(V+65)/20], \\ \beta_h(V) &= \frac{1}{1+\exp[-(V+35)/10]}. \end{aligned}$$

Parameters of the model are as follows: $C = 1\ \mu\text{F/cm}^2$, $V_{\text{L}} = -54.4$ mV, $g_{\text{L}} = 0.3\ \text{mS/cm}^2$, $V_{\text{K}} = -77$ mV, $\bar{g}_{\text{K}} = 36\ \text{mS/cm}^2$, $V_{\text{Na}} = 50$ mV, $\bar{g}_{\text{Na}} = 120\ \text{mS/cm}^2$.

2. Stochastic sensitivity and the Mahalanobis distance

Consider a nonlinear stochastic dynamical system governed by the following stochastic differential equation:

$$\dot{\mathbf{x}} = \mathbf{f}(\mathbf{x}) + \varepsilon \mathbf{g}(\mathbf{x})\boldsymbol{\xi}(t), \tag{A2}$$

where $\mathbf{x}$ is an n-dimensional vector, $\mathbf{f}(\mathbf{x})$ is a smooth n-dimensional vector function, $\boldsymbol{\xi}(t)$ is an n-dimensional Gaussian white noise with $\langle \boldsymbol{\xi}(t)\boldsymbol{\xi}^{\top}(t+\tau)\rangle = \delta(\tau)\mathbf{I}$, $\mathbf{I}$ is an $n \times n$ identity matrix, and $\mathbf{g}(\mathbf{x})$ is an $n \times n$ matrix function of noise intensity.

At first, let us assume that the system (A2) without noise ($\varepsilon = 0$) possesses an exponentially stable equilibrium, $\mathbf{x} \equiv \bar{x}$. Random trajectories of the noisy forced system (A2) leave its equilibrium $\bar{\mathbf{x}}$ and, according to the stability of $\bar{\mathbf{x}}$, form some probabilistic distribution around $\bar{\mathbf{x}}$. The time evolution of this distribution is described by the corresponding Kolmogorov-Fokker-Planck equation [38]. We assume that a stationary (steady-state) solution exists, $\rho(\mathbf{x},\varepsilon)$. Generally, for systems with $n \geqslant 2$ it is hard or nearly impossible to find such stationary probability density analytically [7,38]. In the case of small noise, $\varepsilon \ll 1$, the constructive asymptotics and approximations based on a quasipotential function,

$$\Phi(\mathbf{x}) = -\lim_{\varepsilon \to 0} \varepsilon^2 \log \rho(\mathbf{x},\varepsilon), \tag{A3}$$

are commonly used [8].

A quadratic form of the quasipotential gives a Gaussian approximation of $\rho(\mathbf{x},\varepsilon)$ in a neighborhood of the equilibrium $\bar{\mathbf{x}}$,

$$\rho_G(\mathbf{x},\varepsilon;\bar{\mathbf{x}}) = N \exp\left[-\frac{(\mathbf{x}-\bar{\mathbf{x}})^{\top}\mathbf{Q}^{-1}(\mathbf{x}-\bar{\mathbf{x}})}{2\varepsilon^2}\right], \tag{A4}$$

with the mean $\bar{\mathbf{x}}$, the covariance matrix $\mathbf{C} = \varepsilon^2\mathbf{Q}$, and the normalization constant, N. Here, the matrix $\mathbf{Q}$ is a solution of the following equation:

$$\mathbf{J}\mathbf{Q} + \mathbf{Q}J^{\top} + S = 0, \tag{A5}$$

where $\mathbf{J}$ is the Jacobian of the deterministic system at $\mathbf{x} = \bar{\mathbf{x}}$ and $\mathbf{S} = \mathbf{g}(\bar{\mathbf{x}})\,\mathbf{g}^{\top}(\bar{\mathbf{x}})$. For the exponentially stable equilibrium, $\bar{\mathbf{x}}$, the eigenvalues of the Jacobian matrix, $\mathbf{J}$, have negative real parts, and the matrix equation (A5) has a unique solution being the stochastic sensitivity matrix of the equilibrium [22].

For the quantitative geometrical analysis of noise-induced transitions from the equilibrium $\bar{\mathbf{x}}$ to another attractor across a separatrix, we propose to use the Mahalanobis distance [25],

$$r(\mathbf{x};\bar{\mathbf{x}}) = \sqrt{(\mathbf{x}-\bar{\mathbf{x}})^{\top}\, C^{-1}\,(\mathbf{x}-\bar{\mathbf{x}})},$$

where $\mathbf{C}$ is a covariation matrix of the random states around the equilibrium. Surfaces on which $r(\mathbf{x};\bar{\mathbf{x}})$ is constant are confidence ellipsoids that are centered about the mean $\bar{\mathbf{x}}$.

In the special case in which the coordinates of random states are uncorrelated and the variances in all directions are the same, these surfaces are spheres, and the Mahalanobis distance becomes equivalent to the Euclidean distance. The basic geometric features of the nonuniformity of the spatial distribution of random states around the equilibrium are reflected by the stochastic sensitivity matrix $\mathbf{Q}$. Therefore, we use the Mahalanobis distance in the following form:

$$d_M(\mathbf{x};\bar{\mathbf{x}}) = \sqrt{(\mathbf{x}-\bar{\mathbf{x}})^\top \mathbf{Q}^{-1}(\mathbf{x}-\bar{\mathbf{x}})}.$$

In terms of $d_M(\mathbf{x};\bar{\mathbf{x}})$, the Gaussian probability density function can be presented as

$$\rho_G(\mathbf{x},\varepsilon;\bar{\mathbf{x}}) = N\exp\left[-\frac{d_M^2(\mathbf{x};\bar{\mathbf{x}})}{2\varepsilon}\right].$$

Note that the function $d_M^2(\mathbf{x},\bar{\mathbf{x}})/2$ is the quadratic approximation for the quasipotential $\Phi(\mathbf{x})$. A geometric configuration of the confidence ellipsoid is defined by the eigenvalues λ_i and eigenvectors $\mathbf{v}_i$ of the stochastic sensitivity matrix $\mathbf{Q}$, and noise strength ε.

As an illustration, we calculate the stochastic sensitivity matrix and the Mahalanobis distance for an equilibrium of the 2D FitzHugh-Nagumo equation. Let $(\bar{V},\bar{w})$ be a stable equilibrium of the deterministic FitzHugh-Nagumo system (3). The stochastic sensitivity matrix $\mathbf{Q}$ of this equilibrium is symmetric for the stochastic system (3) with $\varepsilon = \sqrt{2D}$, and it is a solution of Eq. (A5), with

$$\mathbf{J} = \begin{bmatrix} a & -1 \\ 0.1 & -0.08 \end{bmatrix}, \quad \mathbf{S} = \begin{bmatrix} 1 & 0 \\ 0 & 0 \end{bmatrix}, \quad a = 1-\bar{V}^2.$$

The elements of $\mathbf{Q}$ can be found explicitly,

$$q_{11} = \frac{13.3-10a}{20a^2-26.6a+2}, \quad q_{12} = \frac{1}{20a^2-26.6a+2},$$
$$q_{22} = \frac{1.25}{20a^2-26.6a+2}.$$

Using these elements, the Mahalanobis distance is

$$d_M(V,w;\bar{V},\bar{w}) = \sqrt{\frac{(13.3-10a)(V-\bar{V})^2 + 2(V-\bar{V})(w-\bar{w}) + 1.25(w-\bar{w})^2}{20a^2-26.6a+2}}.$$

Now consider the case when the deterministic system (A2), $\varepsilon = 0$, possesses an exponentially stable limit cycle, Γ, defined by a T-periodic solution, $\bar{\mathbf{x}}(t) = \bar{\mathbf{x}}(t+T)$. Let Π_t be a hyperplane transversal to the cycle. For the Poincaré section Π_t in the neighborhood of the point $\bar{\mathbf{x}}(t)$, the Gaussian approximation of the probability density reads [22]

$$\rho_G(\mathbf{x},\varepsilon;\bar{\mathbf{x}}(t)) = N\exp\left[-\frac{[\mathbf{x}-\bar{\mathbf{x}}(t)]^\top \mathbf{Q}^+(t)\,[\mathbf{x}-\bar{\mathbf{x}}(t)]}{2\varepsilon^2}\right]$$

with the mean $\bar{\mathbf{x}}(t)$ and the covariance matrix $\mathbf{C}(t) = \varepsilon^2\mathbf{Q}(t)$ and $t \in (0,T]$. Here the matrix function $\mathbf{Q}(t)$ is singular, and the sign "+" means a pseudoinversion. The matrix $\mathbf{Q}(t)$ characterizes the dispersion of the points of intersection of the random trajectories with Π_t, and it is the stochastic sensitivity function of the limit cycle.

For the exponentially stable limit cycle, Γ, the largest Lyapunov exponent is 0 and the rest are negative. Consequently, the matrix $\mathbf{Q}(t)$ is a unique solution of the Lyapunov equation [22],

$$\dot{\mathbf{Q}} = \mathbf{J}(t)\,\mathbf{Q} + \mathbf{Q}\,\mathbf{J}^\top(t) + \mathbf{P}(t)\,\mathbf{S}(t)\,\mathbf{P}(t), \qquad \text{(A6)}$$

with the conditions

$$\mathbf{Q}(0) = \mathbf{Q}(T), \quad \mathbf{Q}(t)\mathbf{f}[\bar{\mathbf{x}}(t)] \equiv 0.$$

In (A6), $\mathbf{J}(t)$ is the Jacobian of the deterministic system at the limit cycle, $\mathbf{S}(t) = \mathbf{g}[\bar{\mathbf{x}}(t)]\,\mathbf{g}^\top[\bar{\mathbf{x}}(t)]$, and $\mathbf{P}(t)$ is a matrix of the orthogonal projection onto the hyperplane Π_t. Eigenvalues, $\lambda_i(t)$, and eigenvectors, $\mathbf{v}_i(t)$, of the stochastic sensitivity matrix, $\mathbf{Q}(t)$, define a spatial arrangement of the confidence ellipsoid around $\bar{\mathbf{x}}(t)$ for the Poincaré section, Π_t.

The Mahalanobis distance is then defined as

$$d_M(\mathbf{x};\bar{\mathbf{x}}(t)) = \sqrt{[\mathbf{x}-\bar{\mathbf{x}}(t)]^\top\,\mathbf{Q}^+(t)\,[\mathbf{x}-\bar{\mathbf{x}}(t)]}.$$

In the 2D case, the stochastic sensitivity matrix can be written in the form [21] $\mathbf{Q}(t) = \mu(t)\mathbf{P}(t)$, where $\mu(t) = \mu(t+T) > 0$ is a unique solution of the boundary problem,

$$\dot{\mu} = \alpha(t)\mu + \beta(t), \quad \mu(0) = \mu(T),$$

with T-periodic coefficients

$$\alpha(t) = \mathbf{p}^\top(t)\,[\mathbf{J}^\top(t) + \mathbf{J}(t)]\mathbf{p}(t), \quad \beta(t) = \mathbf{p}^\top(t)\,\mathbf{S}(t)\,\mathbf{p}(t),$$

where $\mathbf{p}(t)$ is a normalized vector orthogonal to $\mathbf{f}[\bar{\mathbf{x}}(t)]$. Here, the Mahalanobis distance has a simple representation:

$$d_M(\mathbf{x};\bar{\mathbf{x}}(t)) = \frac{\|\mathbf{x}-\bar{\mathbf{x}}(t)\|}{\sqrt{\mu(t)}}.$$

[1] D. Paydarfar, D. B. Forger, and J. R. Clay, J. Neurophysiol. **96**, 3338 (2006).
[2] G. Cymbalyuk and A. Shilnikov, J. Computat. Neurosci. **18**, 255 (2005).
[3] H. A. Lechner, D. A. Baxter, J. W. Clark, and J. H. Byrne, J. Neurophysiol. **75**, 957 (1996).
[4] G. G. Turrigiano, E. Marder, and L. Abbott, J. Neurophysiol. **75**, 963 (1996).

[5] C. Meunier and A. Verga, J. Stat. Phys. **50**, 345 (1988)
[6] N. G. Van Kampen, *Stochastic Processes in Physics and Chemistry* (Elsevier, Amsterdam, 2007).
[7] C. W. Gardiner, *Stochastic Methods: A Handbook for the Natural and Social Sciences* (Springer, Berlin, 2009).
[8] M. I. Freidlin and A. D. Wentzell, *Random Perturbations of Dynamical Systems* (Springer, Berlin, 1998), Vol. 260.
[9] R. Graham and T. Tél, Phys. Rev. Lett. **52**, 9 (1984).
[10] C. Kurrer and K. Schulten, Physica D **50**, 311 (1991).
[11] M. V. Day, J. Dyn. Dif. Eqs. **8**, 573 (1996).
[12] I. A. Khovanov, A. V. Polovinkin, D. G. Luchinsky, and P. V. E. McClintock, Phys. Rev. E **87**, 032116 (2013).
[13] M. I. Dykman, P. V. E. McClintock, V. N. Smelyanski, N. D. Stein, and N. G. Stocks, Phys. Rev. Lett. **68**, 2718 (1992).
[14] M. Dykman, E. Mori, J. Ross, and P. Hunt, J. Chem. Phys. **100**, 5735 (1994).
[15] R. V. Roy, Int. J. Nonlinear Mech. **32**, 173 (1997).
[16] V. N. Smelyanskiy, M. I. Dykman, and B. Golding, Phys. Rev. Lett. **82**, 3193 (1999).
[17] S. Soskin, J. Stat. Phys. **97**, 609 (1999).
[18] N. A. Khovanova and J. Windelen, Appl. Phys. Lett. **101**, 024104 (2012).
[19] S. Beri, R. Mannella, D. G. Luchinsky, A. N. Silchenko, and P. V. E. McClintock, Phys. Rev. E **72**, 036131 (2005).
[20] G. Mil'shtein and L. Ryashko, J. Appl. Math. Mech. **59**, 47 (1995).
[21] I. Bashkirtseva and L. Ryashko, Physica A **278**, 126 (2000).
[22] I. A. Bashkirtseva and L. B. Ryashko, Math. Comput. Sim. **66**, 55 (2004).
[23] I. Bashkirtseva and L. Ryashko, Phys. Rev. E **83**, 061109 (2011).
[24] I. Bashkirtseva, L. Ryashko, and E. Slepukhina, Fluct. Noise Lett. **13**, 1450004 (2014).
[25] P. C. Mahalanobis, Proceedings of the National Institute of Sciences of India **2**, 49 (1936).
[26] A. L. Hodgkin and A. F. Huxley, J. Physiol. **117**, 500 (1952).
[27] P. Rowat, Neural Computat. **19**, 1215 (2007).
[28] H. C. Tuckwell, J. Jost, and B. S. Gutkin, Phys. Rev. E **80**, 031907 (2009).
[29] H. C. Tuckwell and J. Jost, Physica A **391**, 5311 (2012).
[30] J. Guckenheimer and R. A. Oliva, SIAM J. Appl. Dyn. Syst. **1**, 105 (2002).
[31] D. R. Cox and P. A. W. Lewis, *The Statistical Analysis of Series of Events* (Methun, London, 1966).
[32] B. Lindner and A. Longtin, Proc. SPIE **5114**, 209 (2003).
[33] P. E. Rowat and P. E. Greenwood, Front. Computat. Neurosci. **8**, 111 (2014).
[34] B. Lindner and E. M. Nicola, Phys. Rev. Lett. **101**, 190603 (2008).
[35] A. Dhooge, W. Govaerts, and Y. A. Kuznetsov, ACM Trans. Math. Software **29**, 141 (2003).
[36] B. Ermentrout, *Simulating, Analyzing, and Animating Dynamical Systems: A Guide to XPPAUT for Researchers and Students* (SIAM, Philadelphia, 2002).
[37] G. McLachlan, *Discriminant Analysis and Statistical Pattern Recognition* (Wiley, Heboken, New Jersey, 2004), Vol. 544.
[38] H. Risken, *The Fokker-Planck Equation: Methods of Solution and Applications* (Springer, Berlin Heidelberg New York, 1996).
[39] F. Schweitzer, *Brownian Agents and Active Particles* (Springer, New York, 2002).
[40] W. Ebeling, Condens. Matter Phys. **7**, 539 (2004).
[41] B. Lindner, New J. Phys. **9**, 136 (2007).